



Mobility of NH bonds in DNA-binding protein HU of *Bacillus stearothermophilus* from reduced spectral density mapping analysis at multiple NMR fields

Hans Vis^{a,*}, Constantin E. Vorgias^{b,**}, Keith S. Wilson^{b,***}, Robert Kaptein^a & Rolf Boelens^{a,****}

^a *Bijvoet Center for Biomolecular Research, Utrecht University, Padualaan 8, NL-3584 CH Utrecht, The Netherlands*

^b *European Molecular Biology Laboratory (EMBL), c/o DESY, Notkestrasse 85, D-22603 Hamburg, Germany*

Received 22 September 1997; Accepted 1 October 1997

Key words: DNA-binding protein, heteronuclear NMR relaxation, model-free approach, protein dynamics, rotational diffusion

Abstract

The dynamics of the backbone NH bonds of protein HU from *Bacillus stearothermophilus* (HUBst) have been characterized using measurements of cross-relaxation, longitudinal and transverse relaxation rates ($R_N(H_Z \leftrightarrow N_Z)$, $R_N(N_Z)$ and $R_N(N_{x,y})$) at 11.7, 14.1 and 17.6 T. Linear regression of the values $2R_N(N_{x,y}) - R_N(N_Z)$ with the squared Larmor frequency ω_N^2 has revealed global exchange processes, which contributed on the order of 0.5–5.0 s⁻¹ to the transverse relaxation rate. Subsequently, the experimental values $R_N(N_{x,y})$ were corrected for these exchange contributions. A reduced spectral density mapping procedure has been employed with the experimental relaxation rates and seven values of the spectral density function $J(\omega)$ have been extracted. These spectral densities have been fitted within the framework of the model-free approach. The densities agree well with an axially symmetric rotational diffusion tensor with a diffusion anisotropy D_{\parallel}/D_{\perp} of 1.15, indicating that the flexible arms of HUBst do not significantly contribute to the rotational diffusion. The overall correlation time is 8.9 ± 0.6 ns/rad. The fast internal motions of most of the NH bonds in the core display order parameters ranging between 0.74 and 0.83 and internal correlation times between 1 and 20 ps. For the residues in the DNA-binding β -arms, an extended version of the model function has been used. The slow internal motions show correlation times of 1–2 ns. The concomitant order parameters (0.3–0.6) are lower than those observed on the fast time scale, indicating that the flexibility of the β -arms is mainly determined by the slower internal motions. A substantial decrease of the generalized order parameters in the β -arms starting at residues Arg⁵⁵ and Ser⁷⁴, opposite on both strands of the β -ribbon arms, has been explained as a ‘hinge’ motion. A comparison of the order parameters for free and DNA-bound protein has demonstrated that the slow hinge motions largely disappear when HU binds DNA.

*Present address: Oxford Centre for Molecular Sciences, University of Oxford, South Parks Road, Oxford OX1 3QT, U.K.

**Present address: Department of Biology, Division of Biochemistry and Molecular Biology, Athens University, Panepistimioplis, 15701 Athens, Greece.

***Present address: Department of Chemistry, University of York, Haslington, York YO1 5DD, U.K.

****To whom correspondence should be addressed.

Supplementary material available from the authors: a table containing the measured cross-relaxation, longitudinal and transverse relaxation rates ($R_N(H_Z \leftrightarrow N_Z)$, $R_N(N_Z)$ and $R_N(N_{x,y})$) for protein HU at the B₀ fields 11.7, 14.1 and 17.6 T.

Introduction

Internal mobility and U.K. flexibility of proteins are of great importance for the function of biological molecules. The measurement of ^{15}N and ^{13}C NMR relaxation rates provides a means of probing the local dynamics of ^{15}N - ^1H and ^{13}C - ^1H bonds in proteins (Wagner, 1993). In general, three rates, in particular longitudinal, transverse and heteronuclear cross-relaxation rates, are used to fit motional parameters using the model-free approach proposed by Lipari and Szabo (1982a,b) for the form of the spectral density function (Kay et al., 1989; Clore et al., 1990a; Palmer et al., 1991; Stone et al., 1992). More recently, Peng and Wagner (1992) have developed the spectral density mapping approach, in which values of the spectral density functions of the ^{15}N - ^1H bonds are directly sampled at several relevant frequencies (e.g. 0, ω_{N} , $\omega_{\text{H}} - \omega_{\text{N}}$, ω_{H} and $\omega_{\text{H}} + \omega_{\text{N}}$), independent of an inherent assumption of the form of the spectral density function. Drawbacks of this method reside in the fact that three additional relaxation rates are required and that anomalous behaviour can be expected for the spectral densities at the three highest frequencies (Peng and Wagner, 1992). Recently, a modified approach was introduced, in which three spectral densities at $\omega_{\text{H}} - \omega_{\text{N}}$, ω_{H} and $\omega_{\text{H}} + \omega_{\text{N}}$ were combined to give an averaged spectral density, $\langle J(\omega_{\text{H}}) \rangle$ (Farrow et al., 1995; Ishima and Nagayama, 1995; Lefèvre et al., 1996); the method is termed 'reduced spectral density mapping' accordingly. For one NMR field, three spectral densities are directly provided by this method using the three traditional relaxation rates and without a priori knowledge of a specific motional model.

The reduced spectral density mapping approach, following the procedure of Lefèvre et al. (1996), has been applied to the 19.5 kDa dimeric protein HU from *Bacillus stearothermophilus* (HUBst), which is composed of two identical subunits consisting of 90 amino acid residues. HUBst is a representative member of the homologous family of the type II DNA-binding proteins (DBP II), which are small basic proteins found in bacteria (Drlica and Rouviere-Yaniv, 1987; Nash, 1996). The protein HU and other DBP II proteins bind as dimers to DNA in a non-specific manner, with the exception of two members: the integration host factor (IHF) (Friedman, 1988; Goodman et al., 1990; Mengeritsky et al., 1993) and transcription factor I (TF1) encoded by bacteriophage SPO1 (Green and Geiduschek, 1985; Geiduschek et al., 1990). DBP II proteins have the ability to bend DNA and they

prefer binding to curved or bent DNA structures (for reviews see Lavoie et al. (1996), Nash (1996) and Rice (1997)). HU is possibly involved in organizing bacterial DNA into nucleosomal particles (Pettijohn, 1988; Schmid, 1990), and in vitro HU facilitates the formation of specific higher order nucleoprotein complexes which regulate a variety of DNA transactions (Johnson et al., 1986; Funnell et al., 1987; Flashner and Gralla, 1988; Echols, 1990; Surette and Chaconas, 1992).

The structure of the core of HUBst has been determined by X-ray crystallography (Tanaka et al., 1984; White et al., 1989). More recently, the character of the flexible DNA-binding arms has been analysed by NMR spectroscopy (Vis et al., 1994, 1995). For the core of the protein (residues 2–54 and 75–89), the solution structure (PDB entry: 1HUE) and the previous X-ray structure are very similar. The protein is a symmetric dimer. Three α -helices are found from residues 4 to 14, 18 to 38 and 84 to 89, while a three-stranded antiparallel β -sheet region is found containing residues 41 to 45, 48 to 54 and 75 to 81. The helices and β -sheets form together a closely packed dimeric hydrophobic core, from which two antiparallel β -hairpin arms (residues 55–74) protrude into the solvent. However, the structure of these arms is highly disordered with respect to the hydrophobic core and could only be analysed using NMR data. (^1H , ^{15}N) NOE data showed that the disorder in the β -arms was due to flexibility (Vis et al., 1995). Biochemical and biophysical data obtained for several DBP II proteins indicate that the β -arms are involved in DNA binding (Lammi et al., 1984; Härd et al., 1989; Shindo et al., 1993), as proposed initially by Tanaka et al. (1984). Recently, we have demonstrated from ^{15}N relaxation data that the flexibility of the β -arm of HUBst is substantially, but not completely, reduced in the complex with DNA (Vis et al., 1996).

Here we present a detailed analysis of ^{15}N relaxation rates of free HUBst performed at three different NMR fields. The internal mobility of the backbone NH bonds of HUBst will be characterized in terms of model-free parameters (Lipari and Szabo, 1982a,b), and the effect of anisotropy of rotational diffusion will be analysed (Schurr et al., 1994; Brüschweiler et al., 1995; Tjandra et al., 1995, 1996; Lee et al., 1997). In addition, model-free parameters are compared for free and DNA-bound HUBst using ^{15}N relaxation data at one magnetic field.

Materials and methods

Sample preparation

Cloning of the HUBst gene, overproduction and purification of the protein and the DNA-binding assay were described by Padas et al. (1992). Using this recombination procedure, ^{15}N -labelled HUBst protein was prepared by using $^{15}\text{NH}_4\text{Cl}$ in a minimal medium and purified by employing affinity chromatography on heparin-sepharose and Mono-S FPLC. The purity was over 95% as judged by SDS-PAGE and silver staining. Recombinant ^{15}N -labelled HUBst was as active as the protein purified from *B. stearrowthermophilus* with respect to its DNA-binding properties. For the protein–DNA complex, a 16 bp DNA fragment with the sequence d(CAGGCTTGCAAGCCTG) was used.

NMR spectroscopy

NMR experiments were performed at 311 K with 1.0 mM protein samples in 95% H_2O / 5% D_2O , containing 30 mM KPi buffer at pH 4.6 and 100 mM KCl. NMR spectra were recorded on Varian Unity Plus 500 and 750 and Bruker AMX/2 600 NMR spectrometers which were all equipped with triple-resonance HCN probes with a shielded gradient coil.

^{15}N longitudinal relaxation and heteronuclear ^{15}N - ^1H NOE data sets were recorded as described essentially by Dayie and Wagner (1994), using a train of proton 180° pulses during the T_1 relaxation delay to remove effects of cross-correlation. ^{15}N T_1 data sets were recorded in such a way that the signal intensity decayed to zero as a function of the relaxation delay, allowing a two-parameter exponential fit. In the NOE experiments, protons were saturated during 3.5 s prior to the pulse sequence in order to achieve steady-state intensities. ^{15}N transverse relaxation experiments were recorded by employing a Carr-Purcell-Meiboom-Gill (CPMG) pulse train (Meiboom and Gill, 1958) consisting of cycles of four 180° ^{15}N pulses and a centred 180° ^1H pulse, each cycle with 3.4 ms of duration and the spin-echo period ξ being approximately 0.4 ms. All (^{15}N , ^1H)-correlated inversion recovery pulse sequences utilized pulsed-field gradients for coherence selection and were extended by a pulse scheme for sensitivity enhancement (Cavanagh et al., 1991; Kay et al., 1992). Two-dimensional data sets were acquired as 64 (96 at 750 MHz) hypercomplex t_1 points and 512 complex t_2 points and processed into spectra of 512×2048 real data points. Roughly, the spectral widths were 33.0 ppm and 11.0 ppm in the f_1 and f_2 directions, respectively, with the ^{15}N and

^1H carrier frequencies at 119.1 ppm and 4.75 ppm, respectively. ^{15}N relaxation data sets were recorded at 11.7, 14.1 and 17.6 for free HUBst and at 11.7 T for HUBst in the protein–DNA complex.

The number of scans in ^{15}N T_1 , T_2 and heteronuclear ^{15}N - ^1H NOE experiments at all fields was approximately 64 per t_1 increment. For HUBst bound to DNA, the number of scans was 128 for the heteronuclear NOE experiment. A relaxation times series typically consisted of 8–10 different relaxation delays ranging from 48 to 1800 ms for T_1 and from 6 to 200 ms for T_2 . The recording time of a complete relaxation data set at one magnetic field, including T_1 , T_2 and NOE, was 5–6 days. All 2D spectra were processed using our NMR program package TRITON and analysed using the NMR analysis program ALISON on a Silicon Graphics Indy workstation. Non-linear regression of the T_1 and T_2 relaxation data and fitting of spectral densities to various models was done using in-house developed software. Additional analysis of the anisotropic diffusion properties was done using the programs R2R1 and Quadric (Lee et al., 1997).

Backbone longitudinal and transverse ^{15}N spin relaxation rates, $R_N(N_z)$ and $R_N(N_{x,y})$, were obtained by curve fitting of a two-parameter mono-exponential function through the peak intensities using the Levenburg–Marquardt algorithm to minimize χ_n^2 for each residue n (Marquardt, 1963; Press et al., 1992). The uncertainties of peak intensities, σ , were set equal to the average baseline noise in the spectra. The root-mean-square deviations between the calculated and experimental intensities, $\sigma \sqrt{\chi_n^2}$, were used to assess the uncertainties in the relaxation parameters in a Monte-Carlo analysis with 500 simulated data sets (Palmer et al., 1991; Press et al., 1992). Steady-state heteronuclear Overhauser enhancements are $\eta = (I_{\text{sat}} - I_0)/I_0$, in which I_{sat} and I_0 are cross-peak intensities with and without ^1H saturation, respectively. The average values of η and standard deviations were determined from two independent measurements. Cross-relaxation rates between ^{15}N and its attached amide proton, $R_N(\text{H}_z \leftrightarrow \text{N}_z)$, were calculated using $\eta = (\gamma_{\text{H}}/\gamma_{\text{N}}) \times R_N(\text{H}_z \leftrightarrow \text{N}_z)/R_N(\text{N}_z)$, where γ_{H} and γ_{N} are the gyromagnetic ratios for ^1H and ^{15}N nuclei. Uncertainties in $R_N(\text{H}_z \leftrightarrow \text{N}_z)$ were obtained straightforwardly using error propagation equations.

Results and Discussion

A reduced spectral density mapping approach (Lefèvre et al., 1996) was employed to obtain for each independent NMR field three spectral densities, $J(0)$, $J(\omega_N)$ and $\langle J(\omega_H) \rangle$, from three experimentally determined rate constants, $R_N(N_z)$, $R_N(N_{x,y})$ and $R_N(H_z \leftrightarrow N_z)$. The averaged spectral density $\langle J(\omega_H) \rangle$ in this approach is a combination of three spectral densities, $J(\omega_H + \omega_N)$, $J(\omega_H)$, and $J(\omega_H - \omega_N)$, and samples $J(\omega)$ effectively at a frequency of $0.87\omega_H$ (Farrow et al., 1995). The following matrix equation expresses the relationship between the spectral densities and relaxation rates (Lefèvre et al., 1996):

$$\begin{pmatrix} J(0) \\ J(\omega_N) \\ \langle J(\omega_H) \rangle \end{pmatrix} = \begin{pmatrix} \frac{-3}{F} & \frac{6}{F} & \frac{-36}{10F} \\ \frac{4}{F} & 0 & \frac{-28}{5F} \\ 0 & 0 & \frac{4}{5C_{DD}} \end{pmatrix} \times \begin{pmatrix} R_N(N_z) \\ R_N(N_{x,y}) \\ R_N(H_z \leftrightarrow N_z) \end{pmatrix} \quad (1)$$

where $F = 3C_{DD} + 4C_{CSA}$, with the dipolar coupling constant $C_{DD} = \gamma_H^2 \gamma_N^2 \hbar^2 / r_{NH}^6$ and the constant $C_{CSA} = \Delta^2 \omega_N^2 / 3$ representing relaxation contributions from the interaction of the ^{15}N chemical shift anisotropy with the B_0 field. \hbar is Planck's constant divided by 2π and r_{NH} is the internuclear N–H bond distance, taken as 1.02 Å (Keiter, 1986). The ^{15}N chemical shift anisotropy $\Delta = \sigma_{\parallel} - \sigma_{\perp}$, where σ_{\parallel} and σ_{\perp} are the parallel and perpendicular components of the axially symmetric ^{15}N chemical shift tensor, and Δ is taken here to be constant at -160 ppm (Hiyama et al., 1988). Using these constants, the dipolar constant C_{DD} is 5.41×10^9 (rad/s)² and the constant C_{CSA} is 0.87, 1.25 and 1.95×10^9 (rad/s)² at 11.7, 14.1 and 17.6 T, respectively. The linearity of Equation 1 allows one to assess the propagated uncertainties of the sampled spectral density values, δJ_j , simply by a weighted sum, in quadrature, of the errors determined for the experimental relaxation rates δR_i ,

$$(\delta J_j)^2 = \sum_{i=1}^3 c_{ij}^2 (\delta R_i)^2 \quad (2)$$

in which the weights c_{ij}^2 are the squares of the corresponding matrix elements in Equation 1 (Peng and Wagner, 1992).

The presence of chemical exchange in the fast-exchange regime, where only one (^{15}N , ^1H) correlation is observed per NH bond, produces an additional transverse relaxation term R_{ex} to the experimental value $R_N(N_{x,y})$. This exchange contribution, R_{ex} , depends on the ω_N Larmor frequency and can be written as $R_{ex} = \Phi \omega_N^2$ (Peng and Wagner, 1995). The factor Φ is dependent on the intrinsic rate constant of the exchange process τ_{ex}^{-1} , on the chemical shift differences between and population of participating sites, and on the applied ^{15}N spin-echo period ξ in the CPMG pulse train. R_{ex} is essentially independent of ξ if $\xi \gg \tau_{ex}$ and becomes negligible only if $\xi \ll \tau_{ex}$ (Meiboom, 1961; Deverell et al., 1970; Palmer et al., 1991). The presence of chemical exchange for a residue may be noted by a transverse relaxation rate that is high compared to that of the neighbouring residues. The dependence of R_{ex} on ω_N^2 predicts that such exchange would contribute more at a high B_0 field. To account for ^{15}N conformational exchange, an additional term R_{ex} can be added to Equation 1 (Stone et al., 1992; Mandel et al., 1995). However, if the same NH bond vector experiences both fast local motions, which reduce the value of $R_N(N_{x,y})$, and slow conformational exchange, the interference of two opposite contributions to the $R_N(N_{x,y})$ value may hamper the identification of possible exchange processes. Alternatively, with relaxation data sets available from more than one field, R_{ex} can be obtained from the effective values of $J(0)$ after employing Equation 1 (Farrow et al., 1995; Peng and Wagner, 1995). Similarly, the value $2R_N(N_{x,y}) - R_N(N_z)$ (Habazettl and Wagner, 1995), including R_{ex} , depends linearly on ω_N^2 following

$$2R_N(N_{x,y}) - R_N(N_z) = C_{DD}[J(0) + \frac{3}{2}J(\omega_H)] + [\frac{4\Delta^2}{9}J(0) + 2\Phi]\omega_N^2 \quad (3)$$

This last approach was followed here. The frequency-independent term in Equation 3 comprises the dipolar relaxation, while the coefficient of ω_N^2 is determined by both CSA relaxation and chemical exchange processes, represented by the constants Δ and Φ , respectively. The rate constants $2R_N(N_{x,y}) - R_N(N_z)$ at different B_0 fields are calculated by linear regression using Equation 3. The value of $J(0)$ is obtained from the intercept, assuming that the value of $J(\omega_H)$ is negligible relative to $J(0)$ which is well justified by the data shown in Figure 2. Subsequently, the value Φ is obtained from the slope coefficient by substitution of the obtained value of $J(0)$, assuming that Δ is the same (160 ppm) for all residues. Characterization of

the time scale of chemical exchange processes can be obtained as well at a single B_0 field by performing ^{15}N nuclear magnetic relaxation measurements in the presence of a variable radio frequency (rf) field (Deverell et al., 1970; Szypersky et al., 1993; Nicholson et al., 1995; Akke and Palmer, 1996), but such methods have not yet been applied to HUBst.

Relaxation rates and chemical exchange

The average values of the backbone ^{15}N relaxation rates and the average uncertainties are given in Table 1. Separate values were calculated for the residues in the relatively rigid core and in the more flexible parts of HUBst. Residues not included in further analysis are Lys¹⁹, Val²⁸, Leu⁴⁴ and Phe⁴⁷, which showed severely overlapped signals in the spectra. The high $R_N(\text{H}_Z \leftrightarrow \text{N}_Z)$ and low $R_N(\text{N}_{x,y})$ values for residues in the β -arms with respect to the residues in the core indicate larger contributions to the spectral density function at high frequencies in the β -arms (see below). $R_N(\text{N}_Z)$ at 11.7 T for the core is higher than for the flexible parts, whereas the opposite is observed for the values at 14.1 T, indicating that the isobestic frequency, where the contribution of $J(\omega)$ is independent of the internal mobility, has a value between 50 and 60 MHz. Furthermore, it is apparent that the relaxation rates vary systematically with the B_0 strength, originating from the functional dependence of both $J(\omega)$ and the CSA relaxation contribution, via C_{CSA} in Equation 1, for $R_N(\text{N}_Z)$ and $R_N(\text{N}_{x,y})$. However, the substantial increase of $R_N(\text{N}_{x,y})$ with B_0 , as observed for many residues both in the core and in the β -arms of HUBst, cannot be fully accounted for by such a contribution alone and is most likely due to the presence of chemical exchange processes in the fast-exchange regime. The exchange contributions to $R_N(\text{N}_{x,y})$ were calculated using Equation 3 and Figure 1 shows the values of Φ versus the sequence of HUBst based on the relaxation data for three values of ω_N . For almost all backbone NH bonds, significant exchange contributions are observed with Φ ranging approximately between 0.25×10^{-17} s and 2.5×10^{-17} s, which corresponds to exchange contributions ($R_{\text{ex}} = \Phi \omega_N^2$) of approximately $0.5\text{--}5.0$ s⁻¹. The exchange contribution observed in the β -arms is on average only slightly lower than for the core. The nature of the conformational exchange processes can, however, not be elucidated from these data. Nonetheless, the global exchange processes observed for HUBst may be related to the packing stability of the dimer, which is salt-dependent (Welfle et al., 1992). With the salt

concentration applied (0.1 M KCl), the whole conformation of the HUBst dimer may be subjected to some folding/unfolding transitions which occur on the time scale of the CPMG delay ξ .

The uncertainties in the values of Φ , as indicated in Figure 1, are rather high and corrections of the transverse relaxation rates by subtraction of the exchange contribution consequently provide more accurate, but less precise, values $R_N(\text{N}_{x,y})$. Previously, Peng and Wagner (1995) had reported global exchange contributions, obtained in a similar way for eglin c, ranging between approximately 0.04 and 0.7 s⁻¹.

Spectral density values for backbone NH bonds

After removing the term R_{ex} from $R_N(\text{N}_{x,y})$, the measurements at three independent B_0 fields resulted in seven spectral densities $J(\omega)$ for each backbone NH bond. The mapping of spectral densities has been obtained without any assumption for the motional model of the spectral density function. Figure 2 shows plots of $J(\omega)$ versus the residue number sampled at 0, 51, 61, 76, 435, 522 and 653 MHz, respectively. It is clearly seen in Figure 2 that high values of $J(\omega_H)$ for flexible residues in the β -hairpin arms (residues 55–74) are compensated by a reduced value of $J(0)$ with respect to the rigid part of the protein (residues 2–54 and 75–89), which ascertains a constant integral of $J(\omega)$ for each NH bond. The value $J(0)$ is the average of three individual $J(0)$ values obtained at 11.7, 14.1 and 17.6 T. The rather large uncertainties of $J(0)$ for several NH bonds are caused by the imprecise values of R_{ex} used to correct the experimental transverse relaxation rates. Both values $J(\omega_N)$ and $J(\omega_H)$ decrease for almost all residues with increasing frequencies ω_N and ω_H , respectively. Adequate fits of $J(\omega)$ are therefore expected using the well-known model-free formalism proposed by Lipari and Szabo (1982a,b):

$$J^{\text{mod}}(\omega) = \frac{2}{5} \left(\frac{S_f^2 \tau_m}{1 + (\omega \tau_m)^2} + \frac{(1 - S_f^2) \tau_{\text{ef}}}{1 + (\omega \tau_{\text{ef}})^2} \right) \quad (4)$$

In Equation 4 the motion of the NH bond vector is subdivided into an overall isotropic molecular tumbling contribution with a time constant τ_m , and a contribution accounting for fast internal fluctuations, characterized by the order parameter S_f^2 and the time constant τ_f , with $\tau_{\text{ef}}^{-1} = \tau_m^{-1} + \tau_f^{-1}$. The order parameter S_f^2 is a measure of the degree of spatial restriction of the fast internal motion of the NH bond; isotropic internal dynamics gives $S_f^2 = 0$, whereas lack of internal motion gives $S_f^2 = 1$. It is further assumed that

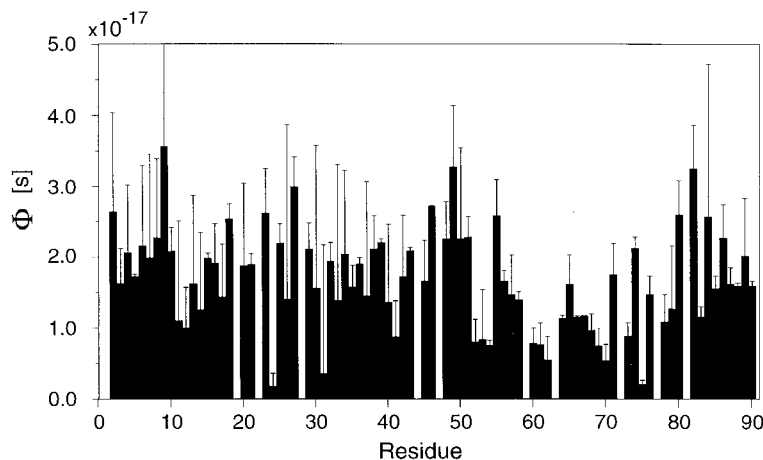


Figure 1. Exchange parameter Φ versus protein sequence. The Φ values are obtained by linear regression using Equation 3 as pointed out in the text. Blank slots indicate prolines or NH bonds which were excluded from the analysis due to severely overlapping NMR signals.

the time scales of the overall and internal motions differ by several orders of magnitude, i.e. $\tau_m \gg \tau_f$. For NH bond dynamics which are unsatisfactorily parametrized using Equation 4, an additional slower internal motion is incorporated in the model with a correlation time τ_s intermediate to the time scales of the fast local motions and of the global molecular tumbling, i.e. $\tau_f < \tau_s < \tau_m$ (Clare et al., 1990b). The extended form of Equation 4 then becomes:

$$J^{\text{mod}}(\omega) = \frac{2}{5} \left(\frac{S_f^2 S_s^2 \tau_m}{1 + (\omega \tau_m)^2} + \frac{(1 - S_f^2) \tau_{ef}}{1 + (\omega \tau_{ef})^2} + \frac{S_f^2 (1 - S_s^2) \tau_{es}}{1 + (\omega \tau_{es})^2} \right) \quad (5)$$

with the effective internal correlation time τ_{es} defined through $\tau_{es}^{-1} = \tau_m^{-1} + \tau_s^{-1}$. The generalised order parameter S^2 , defined as the product $S_f^2 S_s^2$, is a measure of the total amplitude of the internal motions; S_f^2 and S_s^2 are the partial order parameters for the internal motions on the fast and slow time scales, respectively. Note that S^2 equals S_f^2 in Equation 4. A physical interpretation of the correlation times characterizing the internal dynamics requires a theoretical model of motion, such as the wobbling in a cone (Woessner, 1962; Kinoshita et al., 1977; Richarz et al., 1980) or the jump approach (Tropp, 1980).

Order parameters and internal correlation times

The combination of relaxation data sets from three different magnetic fields has resulted in seven independent values of the spectral density function per NH bond, while a maximum of only four parameters using Equation 5 is required to model $J(\omega)$. Therefore, all optimized model-free parameters are considered as

meaningful and no simplification of Equation 4 and especially of Equation 5 will be introduced by assuming that $\tau_f \rightarrow 0$, which is sometimes done when relaxation data are available from one NMR field. In such a case, the lower number of degrees of freedom prohibits obtaining more than three model-free parameters to characterize the internal dynamics.

Good starting values for model-free motional parameters from the experimental spectral densities $J^{\text{exp}}_n(\omega)$ of NH bond n were provided by a coarse and a fine grid search. Subsequently, an iterative non-linear least-squares algorithm (Press et al., 1992) was employed to further minimize the error function χ_n^2 , which is formulated as

$$\chi_n^2 = \sum_{i=1}^{2M+1} (J_n^{\text{exp}}(\omega_i) - J_n^{\text{mod}}(\omega_i))^2 / \delta J_{ni}^2 \quad (6)$$

where δJ_{ni} is defined in Equation 2. The summation runs over $2M + 1$ spectral densities, sampled at frequency ω_i , where M is the number of NMR fields from which relaxation rates are obtained. First, all data were fitted using Equation 4, keeping the three model-free parameters $(\tau_m)_n$, $(S_f^2)_n$ and $(\tau_f)_n$ variable. The overall molecular correlation time τ_m was obtained by averaging the optimized values for all residues which were well parametrized (low χ_n^2) by Equation 4 and showed order parameters higher than 0.70. Thereafter, local model-free parameters were optimized by fixing the optimized value τ_m , using either Equation 4 or Equation 5. Root-mean-square deviations between the predicted and experimental spectral densities were used in a Monte-Carlo procedure to estimate uncer-

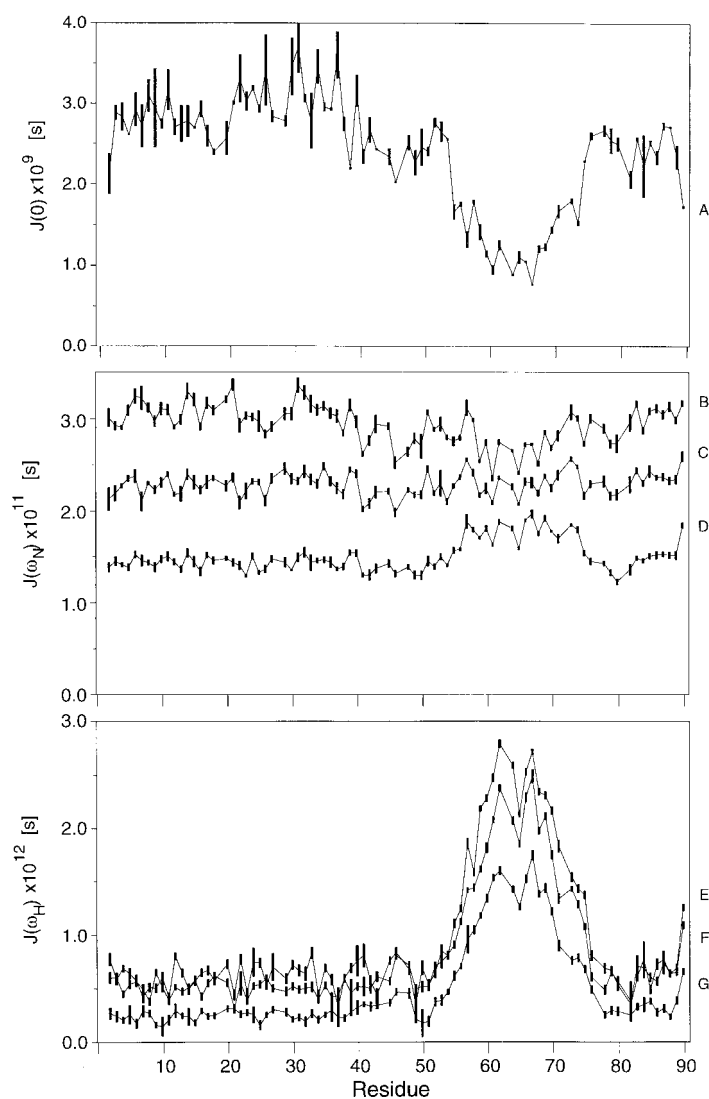


Figure 2. Plots of the spectral density values of backbone NH bonds versus protein sequence. The values (A) $J(0)$, (B) $J(51)$, (C) $J(61)$, (D) $J(76)$, (E) $J(435)$, (F) $J(522)$ and (G) $J(653)$, respectively, are obtained by application of Equation 1 in the text to three experimental ^{15}N relaxation rates measured at three different B_0 fields. $J(0)$ is the average of the results obtained at these three B_0 fields. The values $J(\omega_N)$ and $J(\omega_H)$ both decrease with increasing frequency ω for almost all residues. Uncertainties are indicated by the black vertical bars for each value. The differences of $J(\omega)$ values in the β -arm region (54–75) with respect to the rest of the molecule are indicative of enhanced internal mobility.

Table 1. Average experimental ^{15}N relaxation rates and uncertainties (s^{-1}) for the core and the β -arms (including N- and C-termini) of HUBst at 11.7, 14.1 and 17.6 T

Rate	Core (3–54, 75–89)			β -Arms (2, 55–74, 90)		
	11.7 T	14.1 T	17.6 T	11.7 T	14.1 T	17.6 T
$R_N(N_z)$	1.46 ± 0.03	1.20 ± 0.03	0.85 ± 0.02	1.42 ± 0.03	1.27 ± 0.02	1.07 ± 0.02
$R_N(N_{x,y})$	11.20 ± 0.51	12.29 ± 0.72	14.97 ± 0.35	6.21 ± 0.16	6.75 ± 0.36	8.43 ± 0.12
$R_N(H_z \leftrightarrow N_z)$	0.041 ± 0.004	0.035 ± 0.003	0.018 ± 0.003	0.12 ± 0.01	0.10 ± 0.01	0.07 ± 0.01

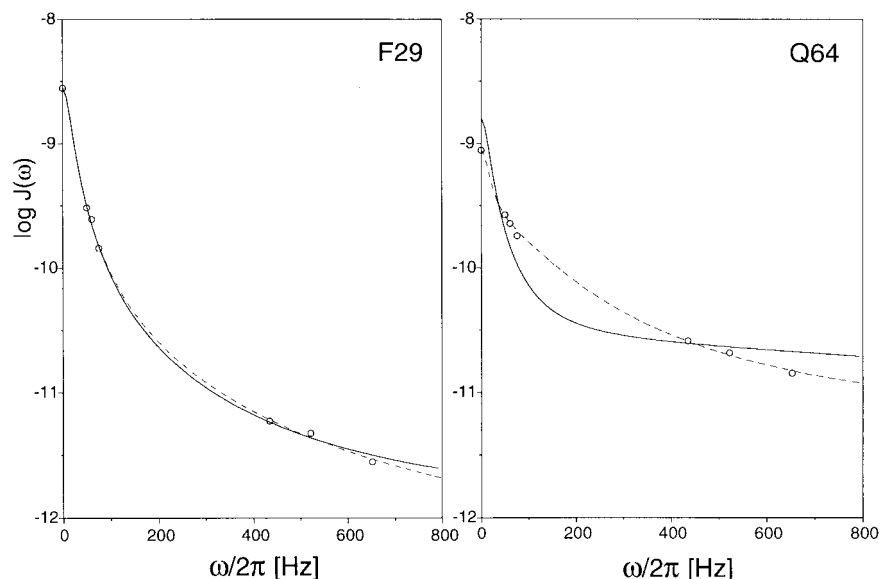


Figure 3. Examples of spectral density functions of residues Phe²⁹ and Gln⁶⁴. Phe²⁹ fits well the model-free formalism of Lipari and Szabo as expressed in Equation 4 (solid curves), whereas Gln⁶⁴ fits much better the extended model-free formalism as expressed in Equation 5 (dashed curves). The sampled spectral density values are indicated as open circles.

tainties in the order parameters and internal correlation times (Palmer et al., 1991).

For HUBst, the mean with standard deviation of the overall isotropic correlation time τ_m thus obtained, using individual values of 54 residues, is 8.9 ± 0.6 ns. After fixing τ_m , the internal dynamics of most backbone NH bonds are satisfactorily parametrized using Equation 4. However, for the β -arms (residues 55–75) and for the residues Lys¹⁸, Gly³⁹, Gly⁴⁶, Glu⁵¹ and Lys⁹⁰, major improvements of χ_n^2 were obtained using Equation 5. Figure 3 shows two examples of the optimized spectral density functions for Phe²⁹ in the core and Gln⁶⁴ in the tip of the β -arm. The improvement of the curve fitting using the extended model function is strikingly visualized for Gln⁶⁴.

Figure 4 shows the generalized order parameters S^2 and the fast-motion order parameters and internal correlation times, S_f^2 and τ_f , as a function of the residue number. In addition, the fitted model-free parameters τ_s and S_s^2 for the residues in the β -arm are presented in Figure 5. Most residues in the core show S^2 values ranging between 0.74 and 0.83, but in the first β -strand (residues 41–44), which is most accessible to the solvent, slightly lower S^2 values of 0.68–0.71 are observed that indicate increased mobility. Gly³⁹ in the turn between α -helix 2 and β -strand 1 is apparently more mobile than its adjacent residues. Order parameters for the fast motions S_f^2 are signif-

icantly lower in the β -arm region than in the core. However, the largest contributions to the low values of the generalized order parameter S^2 are due to the low values of the order parameters for the slow motions S_s^2 .

The fast internal correlation times τ_f for the core residues fluctuate within a range of 1 and 20 ps, with an average value of 16 ps. The residues Asn², Glu⁵, Glu¹², Asp²⁰, Ala²⁴, Thr³³, Asp⁴⁰, Ile⁴⁵, Ala⁸⁴ and Asp⁸⁷, which are all contained in the solvent-exposed parts of the core, show the slowest motions in the core on the fast time scale. Interestingly, the large amplitude motions of the flexible β -arms, which move freely in solution, have substantially longer internal correlation times than the motions of the core residues (see Figure 4C). Apparently, a correlation exists between larger conical angles, indicated by low-order parameters, and longer motional correlation times.

In Figure 4A, the lowest order parameter ($S^2 = 0.14$) is observed for Glu⁶⁷, which is just outside the tip of the β -arm (residues 63–66). Since the β -ribbon arm and especially the turn involving residues Pro⁶³ to Gly⁶⁶ seem to be structured internally (Vis et al., 1995), the drop in S^2 for the β -arm region starting suddenly at residues Arg⁵⁵ and Ser⁷⁴ in the stem of the arm suggests a hinge bending motion about these two residues.

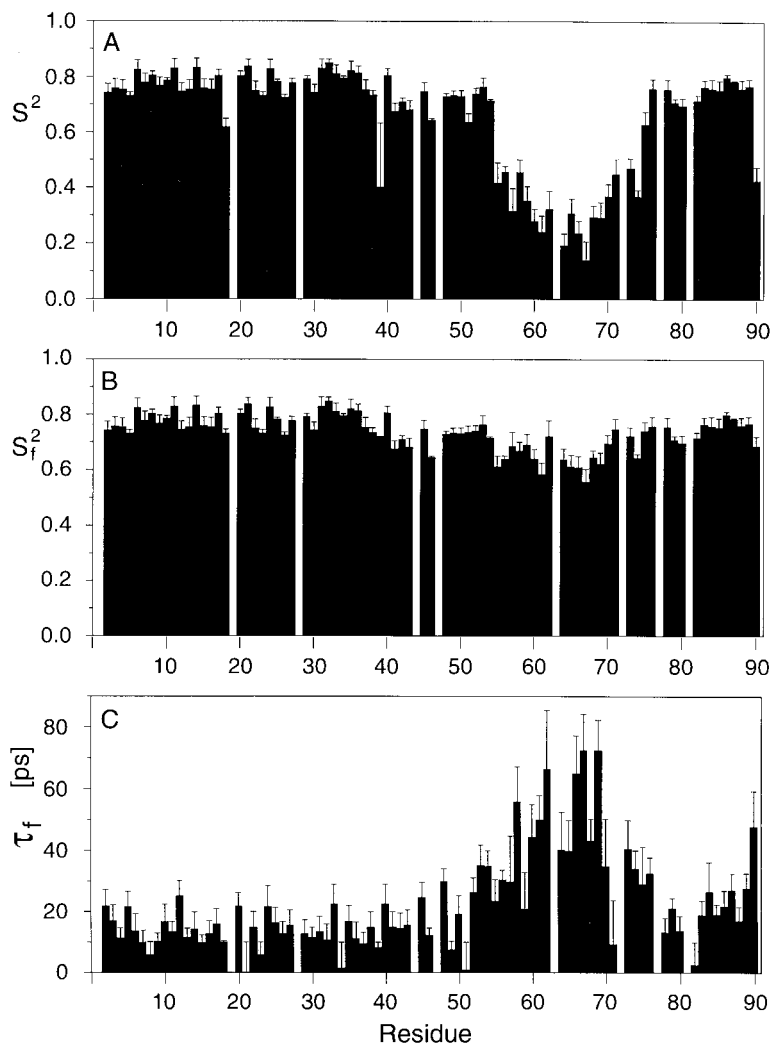


Figure 4. Bar graphs of (A) the generalized order parameter S^2 , (B) the fast-motion order parameter S_f^2 and (C) the fast internal correlation time τ_f versus protein sequence. Values are obtained by fitting spectral densities to Equation 4 or Equation 5. S^2 was calculated as the product $S_f^2 S_s^2$, where the slow-motion order parameter S_s^2 is obtained for residues of which the NH bond dynamics are better characterized by Equation 5. For residues that are well characterized by Equation 4, a value $S_s^2 = 1$ is assumed. A discussion of the values is given in the text.

Anisotropic molecular tumbling for HUBst

From the ensemble of NMR structures of HUBst (Vis et al., 1995), the calculated relative ratio of the principal components of the inertia tensor is 1.0:0.71:0.55 and for the core residues only it is 1.0:0.86:0.72. The anisotropic shape of the symmetric HUBst dimer, which is clearly demonstrated from this ratio, may influence the relaxation behaviour of the NH bonds. The diffusional motion of the protein around the symmetry axis (z-axis), corresponding to the largest component of the diffusion tensor D_z , is expected to be faster than the diffusion around the x- or y-axis, with co-

efficients D_x and D_y . Assuming that the diffusion tensor of HUBst is axially symmetric ($D_x = D_y = D_\perp = (6\tau_\perp)^{-1}$; $D_z = D_\parallel = (6\tau_\parallel)^{-1}$), the geometric dependence on the orientation of the NH bond vector is considerably simplified. The adapted $J^{\text{mod}}(\omega)$ in Equation 4 (Tjandra et al., 1995), accounting for anisotropic molecular tumbling, is then given by

$$J^{\text{mod}}(\omega) = \frac{2}{5} \left(S_f^2 \sum_{k=1}^3 \frac{A_k \tau_k}{1 + (\omega \tau_k)^2} + \frac{(1 - S_f^2) \tau_{\text{ef}}}{1 + (\omega \tau_{\text{ef}})^2} \right) \quad (7)$$

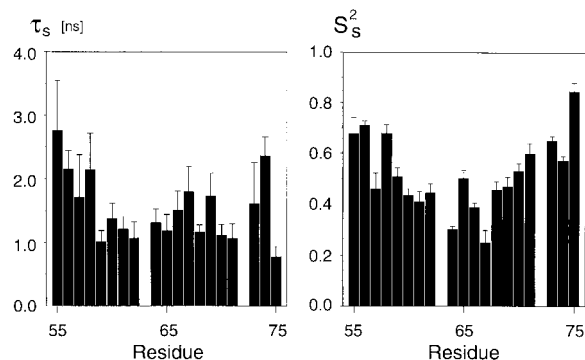


Figure 5. Plots of the slow internal correlation times τ_s and slow-motion order parameters S_s^2 versus the residue number. Values were obtained by fitting spectral densities to Equation 5. The values τ_s are rather constant. Values S_s^2 were shown to be significantly lower than for the core (see Figure 3), but even lower values are shown for S_s^2 in the β -arms of HUBst, and contribute most to the generalized order parameter S^2 .

where $A_1 = (1.5 \cos^2 \alpha - 0.5)$, $A_2 = 3 \sin^2 \alpha \cos^2 \alpha$, $A_3 = 0.75 \sin^4 \alpha$, with α the angle between the NH bond vector and the z-axis, calculated from the molecular structure, and the time constants are $\tau_1 = \tau_{\perp}$, $\tau_2 = 6\tau_{\perp}/\tau_{\parallel}/(\tau_{\perp} + 5\tau_{\parallel})$ and $\tau_3 = 3\tau_{\perp} \tau_{\parallel}/(2\tau_{\perp} + \tau_{\parallel})$. The fast internal correlation time τ_f is still contained in τ_{ef} , but τ_m is substituted by an overall anisotropic tumbling time $\tau_D = (6D)^{-1} = 3\tau_{\perp} \tau_{\parallel}/(\tau_{\perp} + 2\tau_{\parallel})$, D being defined as $1/3$ the trace of the diffusion tensor, $D = 1/3(D_x + D_y + D_z)$. Note that, since $\sum A_i = 1$, replacing both τ_{\perp} and τ_{\parallel} with τ_m simplifies Equation 6 into the isotropic model-free formalism, Equation 4.

From the ratio of the components of the inertia tensor, assuming axial symmetry, the predicted value of D_{\parallel}/D_{\perp} is 1.60 ± 0.05 including all residues and 1.27 ± 0.01 for the core; the difference in the error reflects the structural disorder of the β -hairpin arms. By means of a grid search using Equation 7, the optimal overall time constant τ_D and the ratio D_{\parallel}/D_{\perp} were determined by minimization of the sum over χ_n^2 with the same 54 residues used to determine τ_m . For $\tau_D = \tau_m$ the ratio D_{\parallel}/D_{\perp} was optimized to a value of 1.16 and the improvement of Γ^2 was 5%. A maximum improvement of 16% could be achieved with $\tau_D = 8.6$ ns and $D_{\parallel}/D_{\perp} = 1.15$, and the corresponding time constants τ_{\parallel} and τ_{\perp} are 7.8 and 9.0 ns, respectively.

Analysis of the anisotropic diffusion properties of HUBst through direct fitting of the T_1/T_2 ratios (Tjandra et al., 1995) or through analysis of local diffusion coefficients (Brüschweiler et al., 1995; Lee et al., 1996) gave similar results. For all three different fields the relaxation data of the core of HU

(residues 2–54, 76–89) agree well with an axially symmetric rotational diffusion tensor with $D_{\parallel}/D_{\perp} = 1.30$ and $\tau_D = 8.5$ ns. No significant improvement, as judged from F-statistics, is obtained with a complete anisotropic diffusion model. Similar results are obtained when the relaxation data remain uncorrected for chemical exchange: $D_{\parallel}/D_{\perp} = 1.26$ and $\tau_D = 10.1$ ns. The relaxation data at 17.6 T gave significantly lower χ_n^2 values (up to 50%) when the $R_N(N_{x,y})$ values were first corrected for exchange contributions. In all cases the values of D_{\parallel}/D_{\perp} (1.15–1.30) fit well with the inertia tensor of the core of HUBst with the long principal axis aligned parallel with the symmetry axis of the dimer. The value of D_{\parallel}/D_{\perp} of 1.60, as calculated for a rigid HU molecule including its β -arms, is substantially larger than the experimental values. Apparently, the flexible β -arms do not significantly affect the rotational motion of the molecule.

The approach of directly fitting $J^{\text{mod}}(\omega)$ as described above, which represents all relaxation data, using an axial symmetric rotational diffusion model showed only a modest deviation of the ratio D_{\parallel}/D_{\perp} from 1. Therefore, no further analysis of the experimental ^{15}N relaxation rates has been pursued using a fully anisotropic tumbling model. It should be noted that studies by Tjandra et al. (1995, 1996) have shown that the anisotropy of molecular reorientations has relatively little effect on the order parameters derived from relaxation data.

Comparison of model-free parameters of free and DNA-bound protein

The average experimental ^{15}N relaxation rates $R_N(N_z)$, $R_N(N_{x,y})$ and $R_N(H_z \leftrightarrow N_z)$ measured at 11.7 T for backbone NH bonds of HUBst bound to a 16 bp DNA fragment are $1.12 \pm 0.08 \text{ s}^{-1}$, $14.9 \pm 1.9 \text{ s}^{-1}$ and $0.03 \pm 0.01 \text{ s}^{-1}$, respectively, for the core and $1.25 \pm 0.06 \text{ s}^{-1}$, $11.4 \pm 0.8 \text{ s}^{-1}$ and $0.08 \pm 0.01 \text{ s}^{-1}$, respectively, for the β -arms. Relaxation rates were transformed into three spectral densities $J(0)$, $J(51)$ and $J(435)$ using Equation 1 without taking into account chemical exchange contributions for the values $R_N(N_{x,y})$. Model-free parameters were obtained by fitting the spectral densities with Equation 4, as described above. Exactly the same procedure was followed for the free protein using only the relaxation rates measured at 11.7 T in order to investigate the changes of model-free parameters upon DNA binding.

The overall correlation times τ_m of free and DNA-bound HUBst are 10.0 ± 0.6 ns and 13.3 ± 1.7 ns, respectively, using 60 and 49 core residues with order

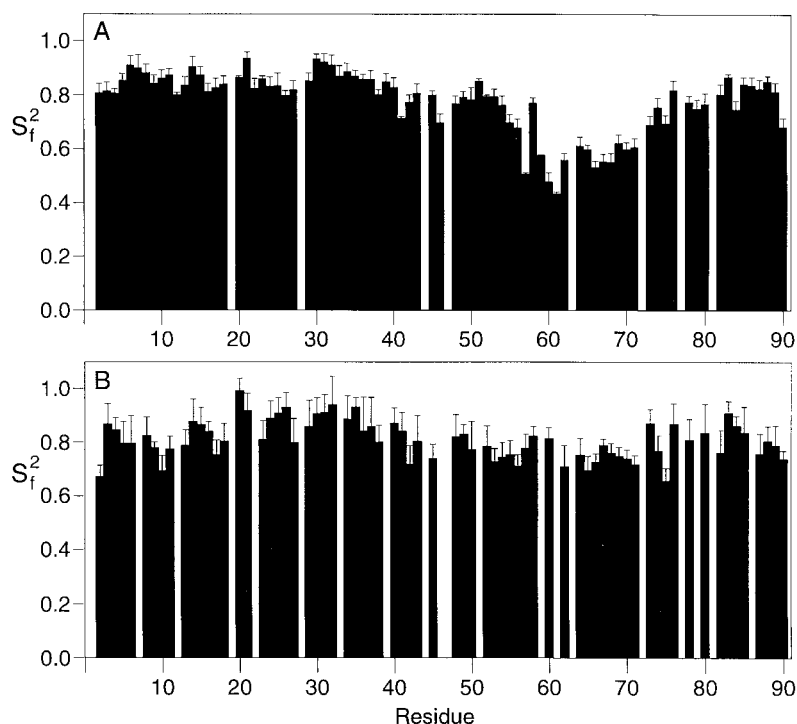


Figure 6. Bar graph of fast-motion order parameters S_f^2 versus protein sequence. Values were obtained using Equation 4 for HUBst both free in solution (A) and in complex with DNA (B). The smaller error bars in (A) with respect to (B) originate from lower experimental uncertainties due to better quality of the spectra recorded for the free protein. Blank slots indicate prolines or NH bonds which were excluded from the analysis due to severely overlapping NMR signals.

parameters S_f^2 larger than 0.7, respectively. The higher τ_m value for the free protein at 11.7 T with respect to the value obtained using data from three magnetic fields is mainly due to not considering chemical exchange effects. Furthermore, the increase of τ_m upon DNA binding reflects the larger molecular size of the protein–DNA complex with respect to free protein. The overall correlation time of DNA-bound HUBst is slightly lower than expected for a complex of 30 kDa, which may be the result of averaging of the relaxation rates due to weak binding of HU to DNA (Vis et al., 1996). With fixed τ_m the spectral densities of the bound protein could all be fitted satisfactorily with Equation 4, yielding low χ_n^2 values for both core and β -arm residues. Also for the core of the free protein, similar low χ_n^2 values were obtained. However, for most residues in the β -arms of the free protein, fitting with Equation 4 yielded about a factor 10 higher χ_n^2 values compared with the values obtained for the core. The poor fits argue for the use of an extended model for the spectral density function and indicate the presence of additional slower motions in the β -arms of the free protein, which have been analysed above.

Figure 6 shows for both free and bound HUBst the order parameters S_f^2 of fast internal motions of the NH bonds versus the protein sequence. With few exceptions, the core residues display order parameters ranging approximately between 0.7 and 0.9 that are not significantly affected by DNA binding. On the other hand, substantial increases of the order parameters for residues in the β -arms occur upon DNA binding. The fast internal correlation times τ_f (data not shown) have similar values for both free and bound protein, with τ_f reaching 60 and 250 ps for the core and the β -arms, respectively. However, the uncertainties of most values of τ_f are very poor, with the relative errors larger than 100%. The results of this comparison demonstrate that the slow sub-nanosecond hinge motions in the β -arms, which dominate the values of the generalized order parameters for the free protein (see Figure 4A), are almost absent when HUBst binds DNA.

Conclusions

In summary, we have measured ^{15}N longitudinal, transverse and heteronuclear NOE relaxation data at three different NMR fields in order to characterize the NH bond mobility along the backbone of HUBst. Global chemical exchange processes have been elicited and accounted for in the transverse relaxation rate values. Seven discrete values of the spectral density function have been determined by means of a reduced spectral density mapping transformation of the relaxation rates, and the model-free approach has been applied to these values. The molecule tumbles with an overall correlation time of 8.9 ± 0.6 ns. From the order parameters and internal correlation times of the NH bonds, we have demonstrated that the flexibility of the DNA-binding β -hairpin arms is mostly governed by the slower internal motions in the sub-nanosecond time scale. Finally, a substantial decrease of the generalized order parameters at Arg⁵⁵ and Ser⁷⁴ has been interpreted as a hinge motion of the β -arms originating from both residues. This sub-nanosecond hinge motion largely disappears when HU binds DNA, which is in agreement with the view that the functional role of the flexibility of the DNA-binding arms of HU is to facilitate interactions of the β -arms with double-stranded DNA.

Acknowledgements

This work was supported in part by the Netherlands Foundation for Chemical Research (SON) with financial support from the Netherlands Organization for Scientific Research (NWO). The authors would like to thank Dr. Geerten Vuister and Dr. Marco Tessari for assisting with setting up the experiments on the Varian 500 spectrometer. They also very much appreciated the invaluable discussions with Frans Mulder concerning the development of the software to analyse relaxation data. The authors thank Dr. A.G. Palmer III for making available the programs R2R1 and Quadric used in the rotational diffusion analysis.

References

- Akke, M. and Palmer III, A.G. (1996) *J. Am. Chem. Soc.*, **118**, 911–912.
- Brüschweiler, R., Liao, X. and Wright, P.E. (1995) *Science*, **268**, 886–889.
- Cavanagh, J., Palmer III, A.G., Wright, P.E. and Rance, M. (1991) *J. Magn. Reson.*, **91**, 429–436.
- Clore, G.M., Bax, A., Driscoll, P.C., Wingfield, P.T. and Gronenborn, A.M. (1990a) *Biochemistry*, **29**, 8172–8184.
- Clore, G.M., Szabo, A., Bax, A., Kay, L.E., Driscoll, P.C. and Gronenborn, A.M. (1990b) *J. Am. Chem. Soc.*, **112**, 4989–4991.
- Dayie, K.T. and Wagner, G. (1994) *J. Magn. Reson.*, **A111**, 121–126.
- Deverell, C., Morgan, R.E. and Strange, J.H. (1970) *Mol. Phys.*, **18**, 553–559.
- Drlica, K. and Rouviere-Yaniv, J. (1987) *Microbiol. Rev.*, **51**, 301–319.
- Echols, H. (1990) *J. Biol. Chem.*, **265**, 14697–14700.
- Farrow, N.A., Zhang, O., Szabo, A., Torchia, D.A. and Kay, L.E. (1995) *J. Biomol. NMR*, **6**, 153–162.
- Flashner, Y. and Gralla, J.D. (1988) *Cell*, **54**, 713–721.
- Friedman, D.I. (1988) *Cell*, **55**, 545–554.
- Funnel, B., Baker, T. and Kornberg, A. (1987) *J. Biol. Chem.*, **262**, 10327–10334.
- Geiduschek, E.P., Schneider, G.J. and Sayre, M.H. (1990) *J. Struct. Biol.*, **104**, 84–90.
- Goodman, S., Yang, C., Nash, H., Sarai, A. and Jernigan, R. (1990) In *Structure and Methods*, Vol. 2 (Eds., Sarma, R.H. and Sarma, M.H.), Adenine Press, New York, NY, pp. 51–62.
- Green, J.R. and Geiduschek, E.P. (1985) *EMBO J.*, **4**, 1345–1349.
- Habazettl, J. and Wagner, G. (1995) *J. Magn. Reson.*, **B109**, 100–104.
- Härd, T., Sayre, M.H., Geiduschek, E.P. and Kearns, D.R. (1989) *Biochemistry*, **28**, 2813–2819.
- Hiyama, Y., Niu, C.H., Silvertown, J.V., Bavoso, A. and Torchia, D.A. (1988) *J. Am. Chem. Soc.*, **112**, 4989–4991.
- Ishima, R. and Nagayama, K. (1995) *Biochemistry*, **34**, 3162–3171.
- Johnson, R., Bruist, M. and Simon, M. (1986) *Cell*, **46**, 531–539.
- Kay, L.E., Torchia, D.A. and Bax, A. (1989) *Biochemistry*, **28**, 8972–8979.
- Kay, L.E., Keifer, P. and Saarinen, T. (1992) *J. Am. Chem. Soc.*, **114**, 10663–10665.
- Keiter, E.A. (1986) Ph.D. Thesis, University of Illinois, Urbana-Champaign, IL.
- Kinoshita, K., Kawato Jr., S. and Ikegami, A. (1977) *Biophys. J.*, **20**, 289–305.
- Lammi, M., Paci, M. and Gualerzi, C.B. (1984) *FEBS Lett.*, **170**, 99–104.
- Lavoie, B.D., Shaw, G.S., Millner, A. and Chaconas, G. (1996) *Cell*, **85**, 761–771.
- Lee, L.K., Rance, M., Chazin, W.J. and Palmer III, A.G. (1997) *J. Biomol. NMR*, **9**, 287–298.
- Lefèvre, J.F., Dayie, K.T., Peng, J.W. and Wagner, G. (1996) *Biochemistry*, **35**, 2674–2686.
- Lipari, G. and Szabo, A. (1982a) *J. Am. Chem. Soc.*, **104**, 4546–4559.
- Lipari, G. and Szabo, A. (1982b) *J. Am. Chem. Soc.*, **104**, 4559–4570.
- Mandel, A.M., Akke, M. and Palmer III, A.G. (1995) *J. Mol. Biol.*, **246**, 144–163.
- Marquardt, D.W. (1963) *J. Soc. Ind. Appl. Math.*, **11**, 431–441.
- Meiboom, S. and Gill, D. (1958) *Rev. Sci. Instrum.*, **29**, 688–691.
- Meiboom, S. (1961) *J. Chem. Phys.*, **34**, 375–388.
- Mengeritsky, G., Goldenberg, D., Mendelson, I., Giladi, H. and Oppenheim, A.B. (1993) *J. Mol. Biol.*, **231**, 646–657.
- Nash, H.A. (1996) In *Regulation of Gene Expression in Escherichia coli* (Eds., Lin, E.C.C. and Lynch, A.S.), R.G. Landes Company, Austin, pp. 149–179.
- Nicholson, L.K., Yamazaki, T., Torchia, D.A., Grzesiek, S., Bax, A., Stahl, S.J., Kaufman, J.D., Wingfield, P.T., Lam, P.Y.S., Jadhav,

- P.K., Hodge, C.N., Domaille, P.J. and Chang, C.H. (1995) *Nat. Struct. Biol.*, **2**, 274–280.
- Padas, P.M., Wilson, K.S. and Vorgias, C.E. (1992) *Gene*, **117**, 39–44.
- Palmer III, A.G., Rance, M. and Wright, P.E. (1991) *J. Am. Chem. Soc.*, **113**, 4371–4380.
- Peng, J.W. and Wagner, G. (1992) *J. Magn. Reson.*, **98**, 308–332.
- Peng, J.W. and Wagner, G. (1995) *Biochemistry*, **34**, 16733–16752.
- Pettijohn, D.E. (1988) *J. Biol. Chem.*, **263**, 12793–12796.
- Press, W.H., Teukolsky, S.A., Vetterling, W.T. and Flannery, B.P. (1992) *Numerical Recipes*, Cambridge University Press, Cambridge.
- Rice, P.A. (1997) *Curr. Opin. Struct. Biol.*, **7**, 86–93.
- Richarz, R., Nagayama, K. and Wüthrich, K. (1980) *Biochemistry*, **19**, 5189–5196.
- Schmid, M.B. (1990) *Cell*, **63**, 451–453.
- Schurr, J.M., Babcock, H.P. and Fujimoto, B.S. (1994) *J. Magn. Reson.*, **B105**, 211–224.
- Shindo, H., Kurumizaka, H., Furubayashi, A., Sakuma, C., Matsumoto, U., Yanagida, A., Goshima, N., Kano, Y. and Imamoto, F. (1993) *Biol. Pharm. Bull.*, **16**, 437–443.
- Stone, M.J., Fairbrother, W.J., Palmer III, A.G., Reizer, J., Saier, M.H. and Wright, P.E. (1992) *Biochemistry*, **31**, 4394–4406.
- Surette, M.G. and Chaconas, G. (1992) *Cell*, **68**, 1101–1108.
- Szyperski, T., Luginbühl, P., Otting, G., Güntert, P. and Wüthrich, K. (1993) *J. Biomol. NMR*, **3**, 151–164.
- Tanaka, I., Appelt, K., Dijk, J., White, S.W. and Wilson, K.S. (1984) *Nature*, **310**, 376–381.
- Tjandra, N., Feller, S.E., Pastor, R.W. and Bax, A. (1995) *J. Am. Chem. Soc.*, **117**, 12562–12566.
- Tjandra, N., Wingfield, P., Stahl, S. and Bax, A. (1996) *J. Biomol. NMR*, **8**, 273–284.
- Tropp, J. (1980) *J. Chem. Phys.*, **47**, 6035–6043.
- Vis, H., Boelens, R., Mariani, M., Stroop, R., Vorgias, C.E., Wilson, K.S. and Kaptein, R. (1994) *Biochemistry*, **33**, 14858–14870.
- Vis, H., Mariani, M., Vorgias, C.E., Wilson, K.S., Kaptein, R. and Boelens, R. (1995) *J. Mol. Biol.*, **254**, 692–703.
- Vis, H., Vageli, O., Nagel, J., Vorgias, C.E., Wilson, K.S., Kaptein, R. and Boelens, R. (1996) *Magn. Reson. Chem.*, **34**, S81–S86.
- Wagner, G. (1993) *Curr. Opin. Struct. Biol.*, **3**, 748–754.
- Welfle, H., Misselwitz, R., Welfle, K., Groch, N. and Heinemann, U. (1992) *Eur. J. Biochem.*, **204**, 1049–1055.
- White, S.W., Appelt, K., Wilson, K.S. and Tanaka, I. (1989) *Proteins*, **5**, 281–288.
- Woessner, D.E. (1962) *J. Chem. Phys.*, **36**, 647–654.